



Simulated ecosystem response to volcanic iron fertilization in the subarctic Pacific ocean

KELLY A. KEARNEY,^{1,*†} DESIREE TOMMASI²
AND CHARLES STOCK²

¹Cooperative Institute for Marine and Atmospheric Studies,
University of Miami Rosenstiel School of Marine and Atmospheric Science, NOAA Atlantic Oceanographic and Meteorological Laboratory, 4301 Rickenbacker Causeway, Miami, FL 33149, USA

²NOAA Geophysical Fluid Dynamics Laboratory, 201 Forrestal Road, Princeton, NJ 08540-6649, USA

ABSTRACT

The eruption of the Kasatochi volcano in August 2008 stimulated an anomalously high phytoplankton bloom in the otherwise iron-limited subarctic Pacific ocean. It has been proposed that this increased production may have been responsible for record returns of some Pacific salmon stocks in the following years. Here, we investigate the potential effect of volcanic-induced iron fertilization on the entire ecosystem, from phytoplankton through to top predators, using a fully-coupled end-to-end ecosystem model. Our simulations indicate that the volcanic iron fertilization could only stimulate modest increases, at most 10%, in the standing stock biomass of upper trophic level species, including fisheries targets such as Pacific salmon. Propagation of energy to higher trophic levels depends on the timing of the eruption, with more efficient crustaceous zooplankton pathways being favored earlier in the growing season and less-efficient gelatinous zooplankton pathways dominating during later months. However, effects were of modest magnitude for all eruption timings, and the strong level of connectivity within the food web makes the preferential stimulation of a single salmon stock implausible. This adds additional support to evidence suggesting that the Kasatochi eruption did not play a large role in subsequent high salmon returns and questions the value of much smaller-scale artificial fertilization for fisheries.

Indeed, the onset of macronutrient limitation coupled with the highly-connected nature of the food web exert strong controls on the fisheries response to even complete removal of iron limitation in the subarctic Pacific.

Key words: end-to-end ecosystem model, iron, Kasatochi volcano, salmon

INTRODUCTION

Iron limits primary production in much of the subarctic North Pacific Ocean, leading to low production and chlorophyll levels despite high concentrations of macronutrients. Iron is supplied to the region primarily through mineral dust deposition (Moore *et al.*, 2002), with some additional transport from coastal regions via mesoscale eddies (Johnson *et al.*, 2005), but surface iron levels typically stay between 0.05 and 0.1 nm.

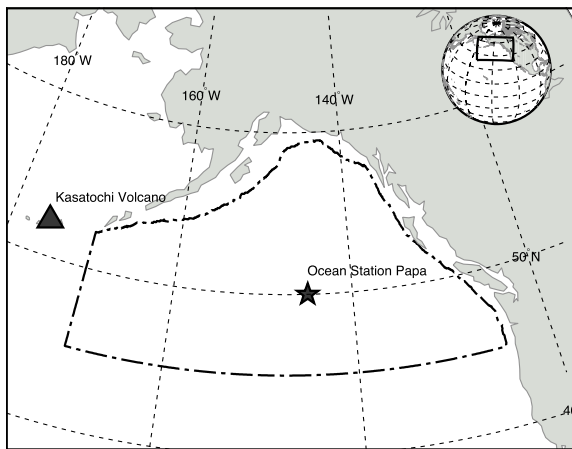
In August 2008, the Kasatochi volcano, located along the southern portion of the Aleutian Islands, erupted, and the resulting ash plume drifted over the Gulf of Alaska region (Fig. 1). Both ship-based and satellite measurements indicated that this led to an anomalously high phytoplankton bloom compared to previous years (Hamme *et al.*, 2010; Langmann *et al.*, 2010). Parsons and Whitney (2012) suggest that this volcano-induced phytoplankton bloom may have been responsible for much higher than average returns of Fraser River sockeye salmon in 2010; they postulate that this particular cohort of salmon would have been migrating into the Gulf of Alaska during the high productivity period. However, McKinnell (2013) counters that survival levels in the 2010 cohort, while higher than the below-average levels seen in the 1990s, were similar to survival rates seen in the preceding decades. He further argues that the increases in diatom and mesozooplankton abundance associated with the eruption would have little effect on juvenile sockeye salmon that would not have been inhabiting the iron-limited portion of the gyre at the time of the eruption. McKinnell (2013) instead attributes the high returns primarily to a high spawner population in 2006.

The idea that iron fertilization could significantly increase fisheries stocks in this region motivated a

*Correspondence. e-mail: kelly.kearney@noaa.gov

†Present address: Joint Institute for the Study of the Atmosphere and Ocean/NOAA Alaska Fisheries Science Center, University of Washington, 7600 Sand Point Way N.E., Building 4, Seattle, WA 98115, USA.

Figure 1. Map of study area. The approximate boundaries of the subarctic gyre region are indicated by the dashed line. Also shown are the locations of the Kasatochi volcano and Ocean Station Papa.



controversial privately-funded fertilization experiment off the coast of Haida Gwaii, British Columbia, during summer 2012 (Tollefson, 2012). As in the case of volcanic fertilization, the excess iron stimulated higher than normal phytoplankton blooms within the Haida eddy in which the iron was dumped (Batten and Gower, 2014; Xiu *et al.*, 2014). However, no direct evidence of higher trophic level responses to either the natural or artificial fertilization events has been measured.

Here, we use an end-to-end ecosystem model that couples physics, biogeochemistry and food web dynamics of the subarctic Pacific food web to further investigate the ecosystem response resulting from a Kasatochi-like iron fertilization event. The model has previously demonstrated skill in reproducing the dominant biogeochemical processes in the region, including seasonal patterns in nutrient cycling, primary production and plankton community composition, while maintaining upper trophic level populations at levels consistent with observations (Kearney *et al.*, 2012). It is thus used here to investigate how volcano-induced primary production may propagate to higher trophic levels, and whether increased salmon returns may be attributed to direct bottom-up food web processes. While the model does not currently focus on the specific life cycle dynamics of the Fraser River salmon cohort, it can provide an estimate of the additional production expected to reach that particular niche in the food web, assuming the salmon were optimally positioned to take advantage of it. More broadly, we investigate the magnitude of the expected fish food web response to the volcanic fertilization event and

the trophic pathways through which energy is likely to travel. We also look at the mechanisms that may damp or amplify the planktonic food web response, and the role of copepod diapause in energy transfer to higher trophic levels.

METHODS

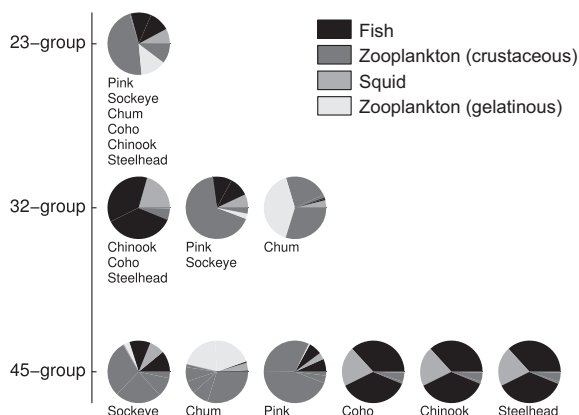
Ecosystem model description

Our simulations were performed using a fully coupled physical, biogeochemical, and ecosystem model. The physical model framework simulates the evolution of a one-dimensional water column, resolved over 50 layers to a 500 m depth with a temporal resolution of 3 h. Advective processes are minimal in this region (Denman and Miyake, 1973), resulting in similar salinity, temperature and nutrient profiles throughout the study area (north of the Subarctic current and excluding the shelf; Wong *et al.*, 2002). Therefore, the water column model captures the primary physical processes that influence primary production in the subarctic gyre region (Fig. 1). The biological component of the model couples traditional NPZ-style (i.e. nutrient, phytoplankton, zooplankton) biogeochemical dynamics, adapted from the NEMURO (Kishi *et al.*, 2007) model, to a food web model derived from the Ecopath with Ecosim (Polovina, 1984; Christensen and Walters, 2004) modeling concept. It explicitly calculates both lower and upper trophic level processes, including primary production, grazing and predation, and fluxes between living organisms and various dissolved and particulate nutrient pools. This model has been previously documented in detail (Kearney *et al.*, 2012, 2013), so here we will give only a brief overview, emphasizing features that have been added to the model framework specifically for this study. A full description of all model equations and parameters can be found in the Supporting information.

The initial conditions and parameter constraints for upper trophic level state variables in this model are derived from the mass balance calculations of an Ecopath model. As in other studies using this fully-coupled model (Kearney *et al.*, 2012, 2013), we used a previously-published Ecopath model for the Eastern Subarctic Pacific (Aydin *et al.*, 2003) as our basis for these parameter constraints. This model, like many Ecopath models developed for fisheries management applications, included a large number of functional groups representing specific managed stocks that occupy very similar niches in the food web. The emphasis of our previous studies was on the main trophic interactions within the food web; a clustering algorithm was thus used to reduce the food web from

45 living functional groups to only 23 living functional groups with distinct trophic characteristics. For this current study, however, we wanted to more fully resolve the different prey pathways to the various salmon species. The Aydin *et al.* (2003) food web includes six salmonid groups: sockeye salmon, chum salmon, pink salmon, coho salmon, Chinook salmon and steelhead. While all salmonid groups feed on a mix of small fish, juvenile squid and zooplankton, the diet compositions vary greatly: chum salmon favor zooplankton, including a large fraction of gelatinous zooplankton, and thus occupy the lowest trophic level of the six groups; sockeye and pink salmon have a diet of three-quarters zooplankton and one-quarter fish and squid; whereas the remaining groups feed almost entirely on fish and squid (Fig. 2, bottom row). In the 23-group simplified food web model, all six of these salmon groups were combined into one, thus losing the distinction between piscivorous and zooplanktivorous prey pathways (Fig. 2, top row). For this study, we chose a lower cutoff value in our clustering process, maintaining three distinct salmon groups and greater diversity within the mesozooplankton community (Fig. 2, middle row). After adding the biogeochemical tracers to this food web, the final ecosystem model includes a total of 40 state variables, encompassing eight nutrient groups (dissolved and particulate nitrogen, silica and iron), two phytoplankton groups, seven zooplankton groups and 23 'nekton' groups (fish, squid, mammals, sharks and birds). Figure 3 depicts all links between these state variables, and a description of the functional groups can be found in Table 1.

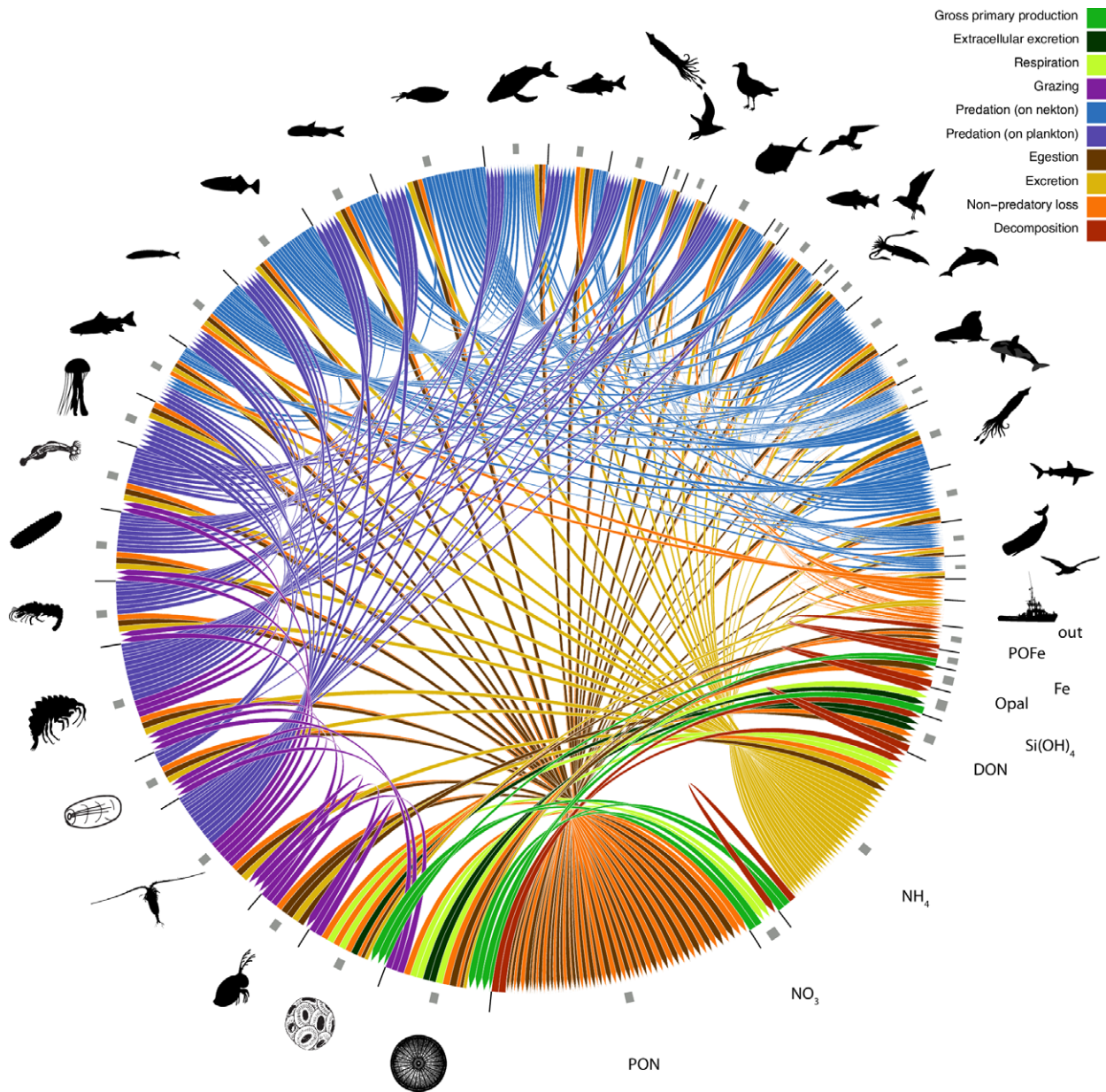
Figure 2. Diet composition of the salmonid groups under various levels of food web clustering. Each slice of the pie represents the fraction of the diet composed of an individual prey group; prey groups are categorized as either fish, zooplankton, or squid.



A diapause option was also added to the equations governing copepod behavior to examine its potential impact on trophic transfer pathways between phytoplankton and salmon. Mesozooplankton biomass in the subarctic Pacific is dominated by large copepods (Miller *et al.*, 1984; Goldblatt *et al.*, 1999) – namely *Neocalanus plumchrus*, *Neocalanus cristatus* and *Eucalanus bungii* – who serve as a major prey source for both pelagic and mesopelagic predators (Aydin *et al.*, 2000). These species all demonstrate ontogenetic migration. In late summer through early autumn, they migrate to depths of ~400–800 m to undergo diapause. Late stage nauplii from the next generation of the *Neocalanus* species and *E. bungii* spawning females migrate back to the surface in the spring (Miller *et al.*, 1984; Mackas *et al.*, 1998). We represented this behavior by splitting the copepod functional group in our model into two subgroups. One includes prescribed directed movement to swim to depths of 400–450 m during the diapause period of each year, and to swim towards the surface at the end of this period; the other group maintains passive movement throughout the year. Under the default parameterization of diapause, transfer from the passive group to the directed movement group occurs over a 20-day period beginning on 1 September, resulting in ~90% of the copepod population moving to the directed movement group, and the entire population is returned to the passive group on 10 April. The 1 September default diapause entry date was selected as an average across the three main copepod species, whose diapause entry varies from August to October (Miller *et al.*, 1984). This model for copepod diapause is similar to those used in other models of North Pacific plankton communities, including the NEMURO model, on which the biogeochemistry of our model is based (Kishi *et al.*, 2001; Aita *et al.*, 2003).

With the addition of the diapause behavior, we also added the option to limit the portion of the water column over which each functional group is able to feed. For this particular food web, we limited pelagic fish and seabird groups to feed on the upper 250 m of the water column; this allows the migrating copepods to escape predation from these particular predators once they have reached their winter depth. The 250 m depth was chosen as a simple midpoint between the copepod's overwintering depth and the deepest depth of the seasonal mixed layer (~100 m), allowing pelagic predators full access to any plankton in the mixed layer but restricting them from the mesopelagic domain. All other nektonic groups were allowed to feed on the entire water column.

Figure 3. A schematic of the biogeochemical and ecological processes connecting all state variables in the model. Edge widths are scaled by the logarithm of the daily flux moving along each link, averaged over 1 year under baseline conditions. The gray boxes along the outside of the circle represent the average biomass of each state variable, using the same scale. State variables are arranged, clockwise from the right, from lowest to highest trophic level.



Our final update to the modeling framework focused on the adsorption of dissolved iron onto particles. Iron scavenging rates have been observed to be elevated above dissolved iron concentrations of 0.6 nM, possibly owing to less complexation with ligands at these concentrations (Johnson *et al.*, 1997). In previous uses of this model, iron levels were maintained at consistently low levels, and therefore we

were able to ignore this effect and use a constant iron scavenging rate. However, in the volcanic fertilization scenario, we expect surface iron concentrations to increase well above this threshold, so we changed the previously-constant iron scavenging rate to reflect the concentration-dependent behavior at higher concentrations. The elevated scavenging rate factor was set to produce an e-folding time of 3–5 days as a result of

Table 1. Ecosystem state variables.

Index	Symbol	Name	Resolution	Includes
1		Albatross	Nektonic, pelagic	Black-footed albatross (<i>Phoebastria nigripes</i>), Laysan albatross (<i>Phoebastria immutabilis</i>)
2		Sperm whales	Nektonic	Sperm whales (<i>Physeter macrocephalus</i>)
3		Sharks	Nektonic	Salmon sharks (<i>Lamna ditropis</i>)
4		Neon flying squid	Nektonic	Neon flying squid (<i>Ommastrephes bartramii</i>)
5		Toothed whales	Nektonic	Orcas (<i>Orcinus orca</i>)
6		Elephant seals	Nektonic	Northern elephant seals (<i>Mirounga angustirostris</i>)
7		Seals, Dolphins	Nektonic	Northern fur seals (<i>Callorhinus ursinus</i>), Dall's porpoises (<i>Phocoenoides dalli</i>), Pacific white-sided dolphins (<i>Lagenorhynchus obliquidens</i>), Northern right whale dolphins (<i>Lissodelphis borealis</i>)
8		Boreal clubhook squid	Nektonic	Boreal clubhook squid (<i>Onychoteuthis borealijaponica</i>)
9		Fulmars	Nektonic, pelagic	Northern fulmar (<i>Fulmarus glacialis</i>)
10		Chinook, Soho, Steelhead	Nektonic, pelagic	Chinook salmon (<i>Oncorhynchus tshawytscha</i>), coho salmon (<i>Oncorhynchus kisutch</i>), steelhead a.k.a. rainbow trout (<i>Oncorhynchus mykiss</i>)
11		Skuas, Jaegers	Nektonic, pelagic	South-polar skuas (<i>Stercorarius maccormicki</i>) and Pomarine jaegers (<i>Stercorarius pomarinus</i>)
12		Pomfret	Nektonic, pelagic	Pacific pomfret (<i>Brama japonica</i>)
13		Puffins, Shearwaters, Storm Petrels	Nektonic, pelagic	Tufted puffins (<i>Fratercula cirrhata</i>), fork-tailed storm petrels (<i>Oceanodroma furcata</i>), Leach's storm petrels (<i>Oceanodroma leucorhoa</i>), sooty shearwaters (<i>Puffinus griseus</i>), short-tailed shearwaters (<i>Puffinus tenuirostris</i>)
14		Kittiwakes	Nektonic, pelagic	Black-legged kittiwakes (<i>Rissa tridactyla</i>)
15		Large gonatid squid	Nektonic	Armhook squid (family Gonatidae)
16		Sockeye, Pink	Nektonic, pelagic	Sockeye salmon (<i>Oncorhynchus nerka</i>), pink salmon (<i>Oncorhynchus gorbuscha</i>)
17		Fin, Sei whales	Nektonic	Fin whales (<i>Balaenoptera physalus</i>), sei whales (<i>Balaenoptera borealis</i>)
18		Micronektonic squid	Nektonic	Juvenile squid, primarily gonatids such as <i>Berryteuthis anonymus</i> and <i>Gonatus onyx</i>
19		Mesopelagic fish	Nektonic	Myctophids a.k.a. lanternfishes (family Myctophidae), particularly <i>Stenobrachius leucopsarus</i>
20		Pelagic forage fish	Nektonic, pelagic	Primarily sticklebacks (<i>Gasterosteus aculeatus</i>)
21		Saury	Nektonic, pelagic	Pacific saury (<i>Cololabis saira</i>)
22		Chum salmon	Nektonic, pelagic	Chum salmon (<i>Oncorhynchus keta</i>)
23		Large jellyfish	Nektonic	Phylum Cnidaria
24		Chaetognaths	Planktonic	Phylum Chaetognatha
25		Predatory zooplankton	Planktonic	Mainly Larvaceans and Polychaetes
26		Sergestid shrimp	Planktonic	Family Sergestidae
27		Other mesozooplankton	Planktonic	Amphipods, pteropods, euphausiids
28		Gelatinous zooplankton	Planktonic	Salps, ctenophores
29		Copepods	Planktonic	Subclass Copepoda
30		Microzooplankton	Planktonic	Any <200 µm, mainly meroplanktonic larva and copepod nauplii
31		Small phytoplankton	Planktonic	Any <5 µm, includes prasinophytes, prymnesiophytes (coccolithophorids), cryptophytes, and cyanobacteria
32		Large phytoplankton	Planktonic	Primarily diatoms
33	PON	Particulate organic nitrogen	Planktonic	
34	NO ₃	Nitrate	Planktonic	
35	NH ₄	Ammmonium	Planktonic	
36	DON	Dissolved organic nitrogen	Planktonic	
37	SiOH ₄	Silicate	Planktonic	

Table 1. (Continued)

Index	Symbol	Name	Resolution	Includes
38	Opal	Particulate opal	Planktonic	
39	Fe	Dissolved iron	planktonic	
40	PoFe	Particulate iron	Planktonic	

The resolution column indicates the ways in which each state variable interacts with the physical model. Planktonic groups are depth-resolved and mix like a passive tracer, while nektonic groups are unaffected by physical mixing. Planktonic groups feed only on groups within the same depth layer as themselves, while nektonic groups feed on the prey field integrated across depth (pelagic groups feed only on the top 250 m).

scavenging, as observed after iron fertilization experiments (Denman *et al.*, 2006). The use of threshold iron scavenging functions is common in global biogeochemical models (Moore *et al.*, 2004) and is supported by detailed mechanistic models run in idealized settings (Fan and Dunne, 2011).

Model scenarios

All simulations were run from 1990 to 2010 using the ECMWF ERA-Interim global atmospheric reanalysis datasets for solar and wind surface forcing. The water column temperature and salinity profiles were initialized with ocean state estimates from ECCO (Version 4 Release 1), a data-assimilating general circulation model. Simulation salinity values were also relaxed to (i.e., nudged towards) the values in this dataset using a 7-day relaxation timescale, allowing the modeled salinity profile to respond to storm events while reflecting the observed seasonal evolution and interannual variability. The first 17 years of the simulations were used for spinup, allowing small drifts in biomass of upper trophic level species (introduced by the seasonal variation at lower trophic levels) to stabilize. Our analysis will focus on the final 3 years (2008–2010) of each simulation.

Several sets of simulations were run. The baseline scenario included a constant surface iron flux of $0.247 \mu\text{mol soluble Fe m}^{-2} \text{ day}^{-1}$, based on dust deposition output from the Geophysical Fluid Dynamics Laboratory Chemical Transport Model (Moxim *et al.*, 2011) with an assumed 3.5% iron content and solubility calculated as described in Fan *et al.* (2006). In the second set of simulations, representing the volcano scenario, this surface iron input value was increased by a factor of 1000 from 9 to 11 August 2008, corresponding to the time period when the volcanic dust cloud traveled over the subarctic gyre region. The factor of 1000 was chosen based on the upper end of estimated iron deposition from the Kasatochi eruption (Langmann *et al.*, 2010); at this level, the model response saturates, so these simulations offer an upper

constraint on the magnitude of the biological response to any surface deposition of iron. On 12 August 2008, the surface iron input in this scenario was restored to its baseline level. To investigate the sensitivity of the ecosystem to the timing of the eruption, we ran two variants with the eruption shifted to 9–11 March and 9–11 June 2008. Observations after the Kasatochi eruption as well as following small-scale patch fertilizations have suggested that copepods may spend more time in surface waters to feed on the increased phytoplankton biomass levels stimulated by fertilization (Hamme *et al.*, 2010; Batten and Gower, 2014), so we included a scenario where copepod diapause was delayed by 3 weeks until 21 September. To account for a scenario in which the diapausing copepod biomass may have been dominated by *Neocalanus plumchrus*, which typically enters diapause earlier in the season (Miller *et al.*, 1984) and thus would not have been present at the time of the eruption, we ran a variant with the diapause cycle beginning on 25 July. Finally, as a theoretical edge case, we also ran a scenario where no copepod diapause occurred at all.

Ensemble parameterization of simulations

As mentioned previously, many of the upper trophic level parameters used in this model are derived from an Ecopath model. The construction of an Ecopath model involves the compilation of a large amount of functional group-related data, including biomass, production rates, consumption rates, diet fractions, growth efficiencies and assimilation efficiencies for each functional group included in the model. These data typically come from a wide variety of sources, ranging from high-quality scientific surveys to fisheries landing data, empirical relationships and other models. The uncertainty values on these numbers can be very high, up to or beyond an order of magnitude from the point estimates, and accurate measurement of these uncertainties is rare. To account for this uncertainty, we assigned each Ecopath parameter a probability distribution based on the best available point

estimate and an uncertainty value ranging from 10 to 80% of that point estimate depending on the quality of the information used to constrain the estimate. One hundred combinations of parameters were then drawn from these probability distributions and used to create an ensemble of 100 different Ecopath models, which were in turn used to parameterize our simulations. The resulting ensemble simulations therefore incorporate the range of results possible given the potential measurement uncertainty in parameters and initial parameterization.

SIMULATION RESULTS

The baseline and volcano scenarios

Under baseline conditions, simulated dissolved iron concentrations in the surface layer range between 0.03 and 0.11 $\mu\text{mol m}^{-3}$, with a mean of 0.07 $\mu\text{mol m}^{-3}$. The increased surface iron deposition under the volcano scenario led to an immediate increase in surface iron concentration, rising to 31.6 $\mu\text{mol m}^{-3}$ over the 2 days of increased input (Fig. 4). The excess surface iron was quickly drawn down as a result of both biological uptake and physical adsorption onto particulate iron. Iron levels dropped to half their maximum after 3 days, and continued to decrease exponentially after this point, returning to pre-fertilization levels approximately 85 days after the eruption.

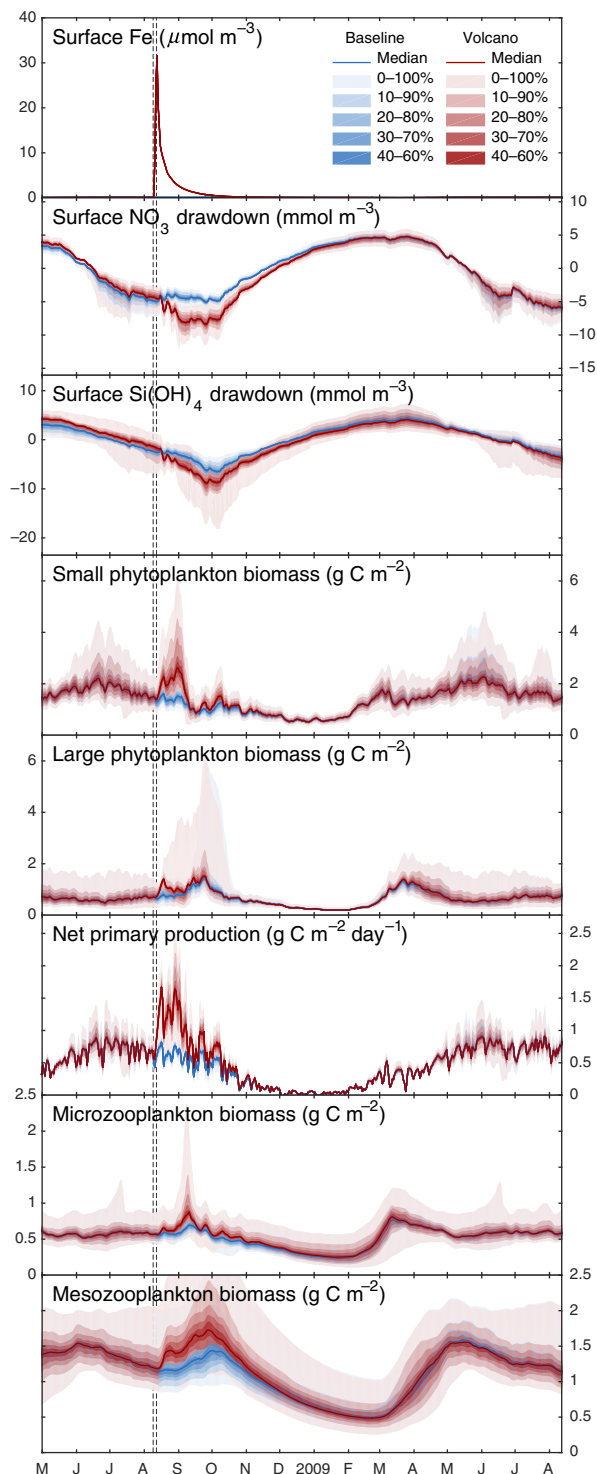
In the standard volcano scenario, both small and large phytoplankton size classes responded to the spike in iron with increases in biomass and production. The small phytoplankton showed a strong initial bloom that began growing immediately after the deposition and peaked on 30 August, (median across ensemble members), 21 days after the eruption, after which biomass levels began to decrease as a result of grazing pressure from the growing micro- and mesozooplankton functional groups (Fig. 4). The time until top-down control is prolonged because microzooplankton accumulation is hindered by predation by mature late-summer mesozooplankton populations at the time of the eruption. The large phytoplankton also experienced a small bloom, but for most ensemble members this initial bloom lasted only a median of 8 days, again reflecting strong top-down control by late summer copepods, gelatinous zooplankton and other crustacean mesozooplankton. A secondary bloom was seen in both phytoplankton size classes in the beginning of September, owing to the alleviation of grazing by dia-pausing copepods. During this secondary bloom, large phytoplankton biomass increased more quickly, with a median peak on 8 September and reached biomass concentrations equal to or greater than (median,

+1.1 mmol N m^{-2}) the earlier bloom. In a few ensemble members, only a single bloom was seen in this size class, with biomass increasing steadily from the time of the eruption until mid-September. The small phytoplankton, who remain tightly grazer-controlled by microzooplankton, experienced only a modest diapause-related bloom, with peak values 10.3 mmol N m^{-2} less than the previous one, and a median peak date of 23 September.

The column-integrated net primary productivity in our simulations reflects the same temporal pattern seen in satellite-derived calculations of net primary productivity over the 2008–2010 time period, with baseline values well within the interannual variability of production values measured at Ocean Station Papa (Fig. 5). Under the volcano scenario, primary productivity rises to approximately twice its baseline value in August 2008 and remains elevated through to September 2008. As the season progresses, decreasing light levels limit production in both the baseline and volcano scenarios, and by November, production in the volcano scenario has returned to baseline levels.

The extra primary production stimulated by the iron fertilization quickly propagates through the food web (Figs 6 and 7). Microzooplankton and copepods see short-lived increases in biomass, with elevated population levels lasting approximately a month before dropping again as a result of grazing pressure, and in the case of copepods, seasonal migration to depth (Fig. 7). The larger zooplankton groups experience more prolonged increases in their populations, rising more gradually and persisting longer than the blooms seen in the phytoplankton and small zooplankton groups; these larger zooplankton groups peak around 1.5 times higher than their baseline counterparts. The trend of more delayed, more prolonged, but smaller magnitude increases in biomass continues as production moves upward through the fish and squid species of the food web. The largest increases in biomass amongst the upper trophic level groups are seen in those who can feed on gelatinous zooplankton (Fig. 8); large jellyfish and chum salmon are the primary beneficiaries here, and the other two salmon groups also benefit. However, even in these groups augmentation of biomass and production in the volcano scenario relative to the baseline scenario generally stays below 30%, with other groups, including sockeye salmon, generally ~10% or less. Owing to their slow growth rates relative to the short pulse of extra production, the homeothermic groups in the food web (marine mammals, birds and sharks) show very little difference in their biomass between the baseline and volcanic scenarios.

Figure 4. Response of nutrient, phytoplankton, and zooplankton state and diagnostic variables to the simulated eruption. Model results are presented as percentile ranges across the 100 ensemble members from each set of simulations. The mesozooplankton panel shows the sum over the copepods, gelatinous zooplankton and other mesozooplankton groups.



It should be noted that in food web models such as this one, growth and reproduction processes are combined into a single growth term, balanced by a loss term. Lower trophic level species, such as microzooplankton and smaller-bodied copepods, have reproductive cycles on the order of days to weeks, and therefore biomass fluctuations at these trophic levels reflect changes in both number and size of individual zooplankton. For higher trophic level organisms with discrete reproduction pathways, such as salmon in this study, the within-year changes are interpreted as reflecting increases in the size of individual fish alongside losses as a result of predation; for these species, we focus more closely on the energy and biomass reaching a group over an annual to multi-year period, rather than the specific within-year patterns of biomass.

Sensitivity to eruption timing

The Kasatochi eruption occurred approximately 2 months after the more productive summer period. At this time of year, light levels have decreased enough to begin limiting phytoplankton growth, and a month later falling temperatures also contribute to lowering the maximum possible growth rate for phytoplankton. Therefore, the resulting bloom stimulated by any alleviation of iron limitation at this late date can only last a short period of time before being countered by light and temperature limitation (Fig. 9).

Eruptions occurring earlier in the growing season allow the small phytoplankton group, which is iron-limited in the spring and summer under baseline conditions, to better capitalize on the increased surface iron input. Both the early spring and summer eruption scenarios alleviate iron limitation enough to allow the small phytoplankton to increase their biomass and productivity over baseline conditions for nearly 3 months before iron levels are reduced to similar-to-baseline limiting levels. A summer eruption is more advantageous for small phytoplankton than an early spring eruption. Small phytoplankton are more nutrient limited during the summer months, but both light and temperature are at their highest levels. This allows the small phytoplankton to maximize their growth rates to the point that they draw down surface nitrogen to limiting levels. With the spring eruption, despite higher macronutrient levels in the spring, the lower light and temperature values lead to a cumulative-over-time production level similar to that seen in the fall eruption (5% higher than baseline), whereas the summer eruption leads to a 10% increase in small phytoplankton net production (Fig. 6).

Large phytoplankton, assumed to be diatoms in our model, are generally more strongly limited by other

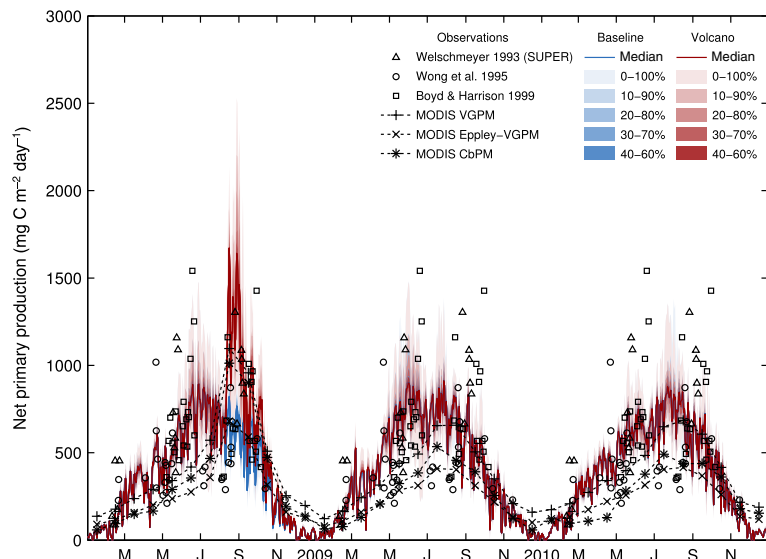


Figure 5. Simulated vs. observed column-integrated production at Ocean Station Papa (50°N , 145°W). Observations include historical measurements collected between 1978 and 1996 as compiled by Boyd and Harrison (1999; displayed here repeated over each year to represent a climatological comparison to the baseline scenario) as well as monthly satellite-derived production for the 2008–2010 period. Model results are presented as percentile ranges across the 100 ensemble members from each set of simulations.

macronutrients than small phytoplankton, and therefore are less able to take advantage of the eruption, regardless of its timing. In the spring eruption scenario, silica limitation prevents a bloom immediately after the iron fertilization, although large phytoplankton were able to bloom briefly approximately 1 month later when deeper mixing owing to a storm increased surface macronutrient levels. Similarly, during the summer eruption, large phytoplankton are able to briefly increase their production levels, but falling nitrogen levels limit their growth more severely than the small phytoplankton with whom they are competing for nutrient uptake. In all scenarios, including the baseline scenario, large phytoplankton experience a secondary bloom late in the year due to copepod diapause. This secondary bloom is largest for later eruptions, when large phytoplankton can benefit from the combination of elevated surface iron levels, lowered grazing pressure from copepods and a competitive advantage over small phytoplankton whose populations remain under pressure from their microzooplankton predators.

Although the total net primary production is highest during a summer eruption, the higher trophic level species benefit more strongly from the early spring eruption. The early spring eruption favors energy pathways that move through the crustacean zooplankton groups, which pass energy more efficiently to higher trophic levels than the gelatinous zooplankton pathway. As a result, a spring eruption increases sockeye salmon biomass levels by a median of 10% over baseline, whereas the summer and fall eruptions provide only 4 and 5% increases, respectively (Fig. 6). Gelatinous zooplankton typically dominate the zooplankton

population later in the year, peaking in October after all other zooplankton groups have begun declining. Therefore, gelatinous zooplankton are able to take full advantage of the later eruptions; their few predators, namely chum salmon and large jellyfish, are likewise able to benefit strongly owing to lack of competition along this food pathway (Figs 6 and 7).

Sensitivity to copepod diapause variations

McKinnell (2013) hypothesized that the copepod migration to depth before or shortly after the August eruption would restrict the transfer of energy to higher trophic levels. Following this logic, we expected higher energy transfer in the delayed-diapause and no-diapause scenarios. However, our simulations demonstrate the opposite results: if copepods delay their migration, net production levels for copepods themselves are increased, but the resulting biomass at higher trophic levels, including the salmon groups, is lower than in the default volcano scenario. With diapause completely eliminated, this pattern is accentuated, with even higher copepod net production but upper trophic biomass levels that are much lower, in some cases even lower than the baseline scenario. The early diapause scenario shows the opposite effect; the copepod group, a majority of which is still actively leaving the surface layer at the time of the eruption, experiences production levels similar to the baseline scenarios, but the energy reaching most upper trophic level groups is higher than the other diapause variant scenarios.

The explanation for this result lies in the strong top-down control on large phytoplankton by abundant mesozooplankton (copepods, gelatinous and other

Figure 6. Biomass and net production ratios, averaged over 2008–2010, for each living state variable, relative to the baseline scenario. Boxplots indicate the range across the 100 ensemble members.

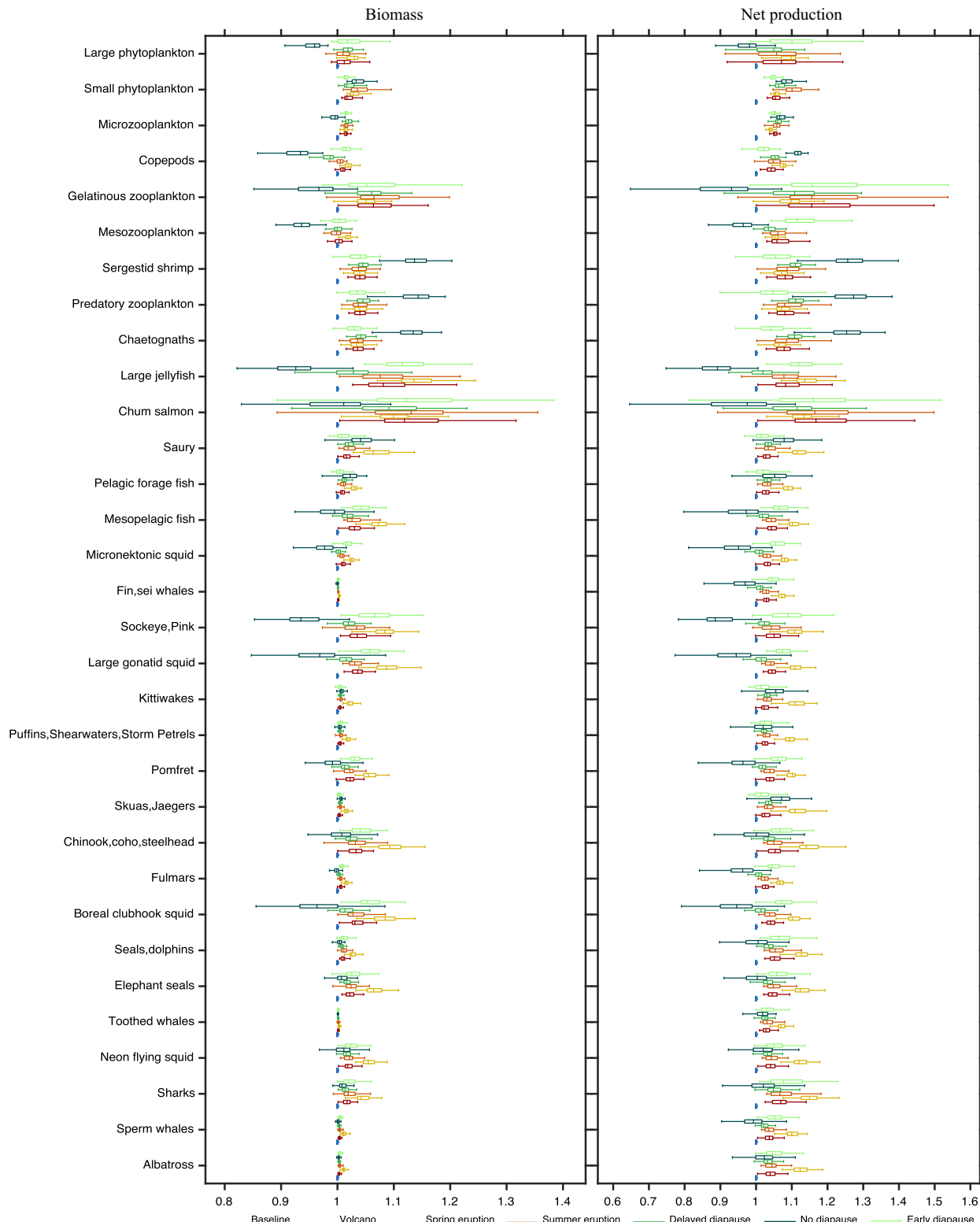


Figure 7. Timeseries of median biomass (across ensemble members) for each scenario. Vertical axes are in units of mmol N m^{-2} and range from 0 to twice the median yearly biomass under baseline conditions for each functional group.

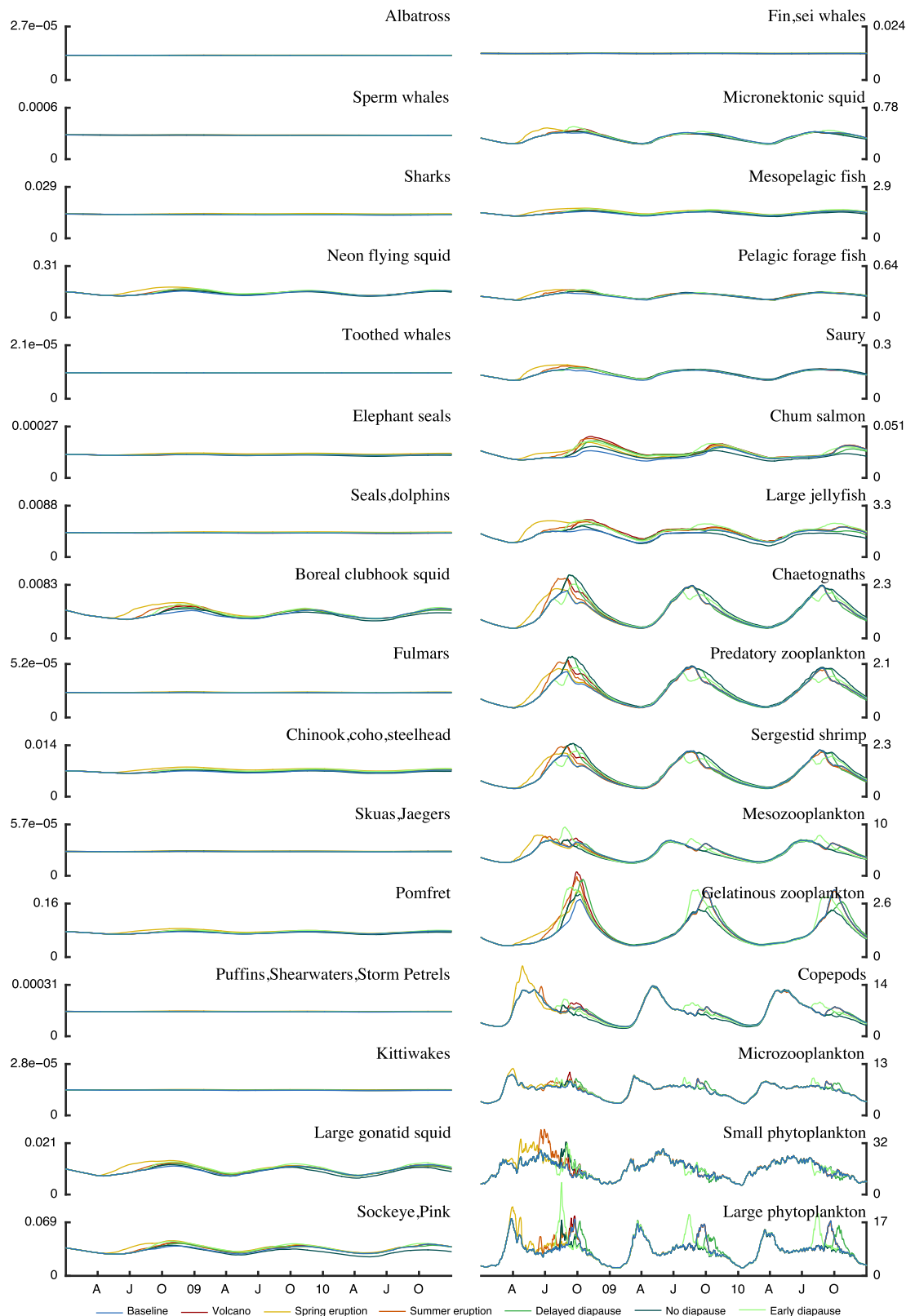
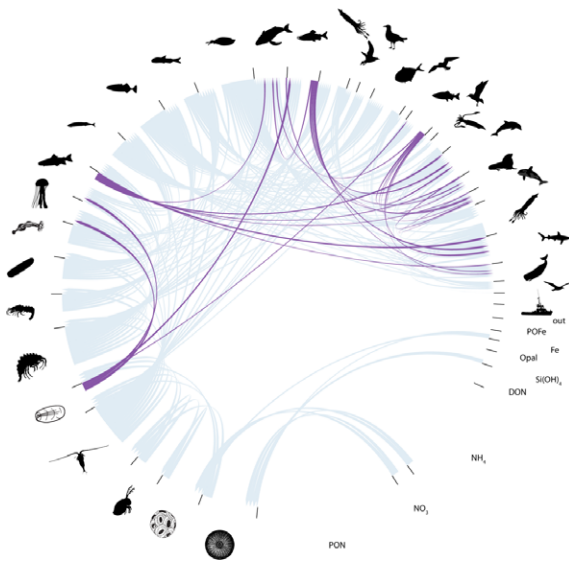


Figure 8. Pathways between gelatinous zooplankton and their predators. Light blue edges indicate links associated with primary production, grazing, and predation; purple edges are those leading up the food web from gelatinous zooplankton.



mesozooplankton) in the North Pacific during the late summer and fall. This grazing pressure hinders the large phytoplankton response to iron fertilization and, through simultaneous controls on microzooplankton, stimulates the small phytoplankton response. Taking copepods away reduces top-down control of large phytoplankton, allowing them to expand in response to fertilization while also allowing microzooplankton to exert tighter controls on small phytoplankton. The result is a shorter, more efficient food web from large phytoplankton through the larger zooplankton groups that remain at the surface following copepod diapause. The top-down control mechanism seen here is similar to that invoked to explain the lack of a pronounced phytoplankton bloom in the region prior to the iron hypothesis (Frost, 1987). When the switch to this more efficient pathway is delayed, as in the delayed diapause scenario, the overall higher trophic level productivity is reduced, as the large phytoplankton productivity feeding into the pathway drops as time between the eruption and the diapause event increases. In the no-diapause scenario, the shift towards the more efficient pathway does not occur, leading to lower biomass of the other mesozooplankton group than is seen in the other simulations. In this scenario, a few of the larger zooplankton groups that compete with other mesozooplankton for food (sergestid shrimp, predatory zooplankton and chaetognaths)

graze on copepods at much higher rates, but these three groups have high non-predatory losses (Fig. 10), and therefore pass only a small fraction of the excess production to their predators. The net effect across the ecosystem is lowered biomass and production levels reaching the upper trophic level groups. Under the early diapause scenario, the volcano-stimulated and predation-reduction large phytoplankton blooms are merged into one, with energy transfer bypassing the copepod group in favor of the other mesozooplankton pathway; the mean biomass and production levels at upper trophic levels under this scenario are very similar to the original volcano scenario, although with higher variance across ensemble members.

DISCUSSION

Despite the large response in lower trophic level groups to the increased surface iron concentrations, our simulations suggest that most upper trophic level groups, including the sockeye/pink salmon functional group, would experience only very modest increases in biomass and production as a result of a volcanic fertilization event. In a few ensemble member simulations, the sockeye/pink group reaches biomass levels approximately twice that of their yearly-averaged baseline counterparts, but the majority see less than a 10% increase over their base values.

The lack of a strong response in the salmon group in this model can be attributed to several factors. The primary reason is the high connectance of the food web, with many groups sharing common prey and predators. In order for salmon biomass to increase significantly, they would need at least a small window of time where their input fluxes greatly outpace their output fluxes, that is, a time when their prey availability increases while their predators (and to a lesser extent, their competitors) maintain the same baseline per capita feeding rates. At the bottom of the food web, this dynamic is possible and leads to the observed population increases in phytoplankton and small zooplankton because production passes in a somewhat step-wise manner from phytoplankton through microzooplankton, copepods, gelatinous and other mesozooplankton, and finally the three larger zooplankton groups. The same type of increases can be seen in the gelatinous zooplankton food chain, where only a small number of groups are able to feed upon the higher than average gelatinous zooplankton population. As a result, the large jellyfish and chum salmon groups are able to outpace their predators and reach peak biomass levels that are twice their typical level (median across ensemble members), and in

some ensemble members up to six times their baseline. However, the pink/sockeye salmon group shares all of its prey groups (other mesozooplankton, pelagic forage fish, mesopelagic fish, micronektonic squid, gelatinous zooplankton, copepods, and predatory zooplankton) with several other functional groups (Fig. 11). Six of their prey groups also serve as prey to at least one of the sockeye salmon's direct predators, and all groups along the pathway from phytoplankton to pink/sockeye salmon are heavily grazed upon by a large number of functional groups, including both predators and competitors of the salmon (Fig. 10). Only a small portion of the increased primary production reaches the sockeye salmon group, and the increased production is simultaneously reaching many other groups in the food web. As a result, sockeye salmon never experience the required window of opportunity where their growth rates could greatly outpace their loss rates and result in an increased standing stock of biomass.

Another sink of excess biomass and production along the route from nutrients to salmon is non-predatory loss. In particular, predatory zooplankton, chaetognaths and mesopelagic fish show a very high fraction of their production going toward non-predatory losses rather than being passed up the food web via predation. The non-predatory loss process is used to represent the net effect of a diversity of loss processes, including natural mortality (i.e., death as a result of old age), loss to disease and viruses, unresolved intra-group mortality (such as egg cannibalism and predation on juveniles of similar species), aggregation and sinking out of the modeled system (primarily applicable to large phytoplankton) and metabolic costs. The parameter values for non-predatory loss rate are derived from the Ecopath model used in the initial parameterization of this model, representing the total production from each prey group that is left over after fulfilling the feeding rates of their predators. The high non-predatory losses may stem from a variety of processes. The low energy density of gelatinous zooplankton translates to a high non-predatory loss because the model assumes similar stoichiometry between all groups. High rates in other groups, such as mesopelagic fish, may be the result of multiple trophic levels being encompassed by a single group. In this case, all intra-group trophic transfer losses would be bundled into the non-predatory loss terms. Finally, groups representing mid-trophic species such as larger zooplankton and small non-target fish species tend to be the least constrained by data. In these cases, the high non-predatory loss rates may indicate missing knowledge regarding the feeding links in the food web. Improved

constraints on non-predatory losses and their dynamics (Kearney *et al.*, 2013) would help refine trophic transfer estimates.

McKinnell (2013) hypothesized that copepod diapause would provide yet another barrier to the propagation of iron fertilization-induced primary production to higher trophic levels, but this did not occur in our simulations. While copepods serve as a prominent grazer of both small and large phytoplankton for most of the year, our model suggests that their migration out of the surface waters coupled with abundant micronutrient concentrations allows for an increase in large phytoplankton production that is efficiently transferred to higher trophic levels by both the other mesozooplankton group and the quick-growing smaller copepods that remain in the surface waters.

Our results highlight the complex balance of micronutrient, macronutrient and top-down influences that determine whether small or large phytoplankton are stimulated. The complexity of responses herein mirror those found in iron fertilization experiments in the North Pacific and elsewhere (Boyd *et al.*, 2004; Takeda and Tsuda, 2005; Uematsu *et al.*, 2009). However, our results do favor stimulation of small phytoplankton over diatoms to a degree greater than suggested by several experiments (Boyd *et al.*, 2004; Tsuda *et al.*, 2005) and by Hamme *et al.*'s (2010) analysis of the plankton response to Kasotochi. This is due to prominent top-down and macronutrient controls on large phytoplankton in the model. However, we note that even the less pronounced diatom bloom created a silica drawdown similar to that observed by Hamme *et al.* (2010). In addition, the preferential stimulation of diatoms was not observed in all iron fertilization experiments (Suzuki *et al.*, 2009). Furthermore, strong top-down control of large phytoplankton is consistent with observations of Continuous Plankton Recorder (CPR) phytoplankton biomass after the privately-funded fertilization off Haida Gwaii, where values were at a historical low, supposedly because of efficient grazing by zooplankton (Batten and Gower, 2014), and with observations during the SEEDS in-situ iron fertilization experiment showing comparable primary production and community grazing rates three weeks after fertilization (Tsuda *et al.*, 2006). The early-diapause simulations did provide a scenario with a prominent diatom response; while this variation enhanced the transfer of energy to higher trophic levels, changes were not enough to impact the overall conclusions of the study.

The simulated increase in copepod production observed across scenarios also appears consistent with North Pacific fertilization experiments responses

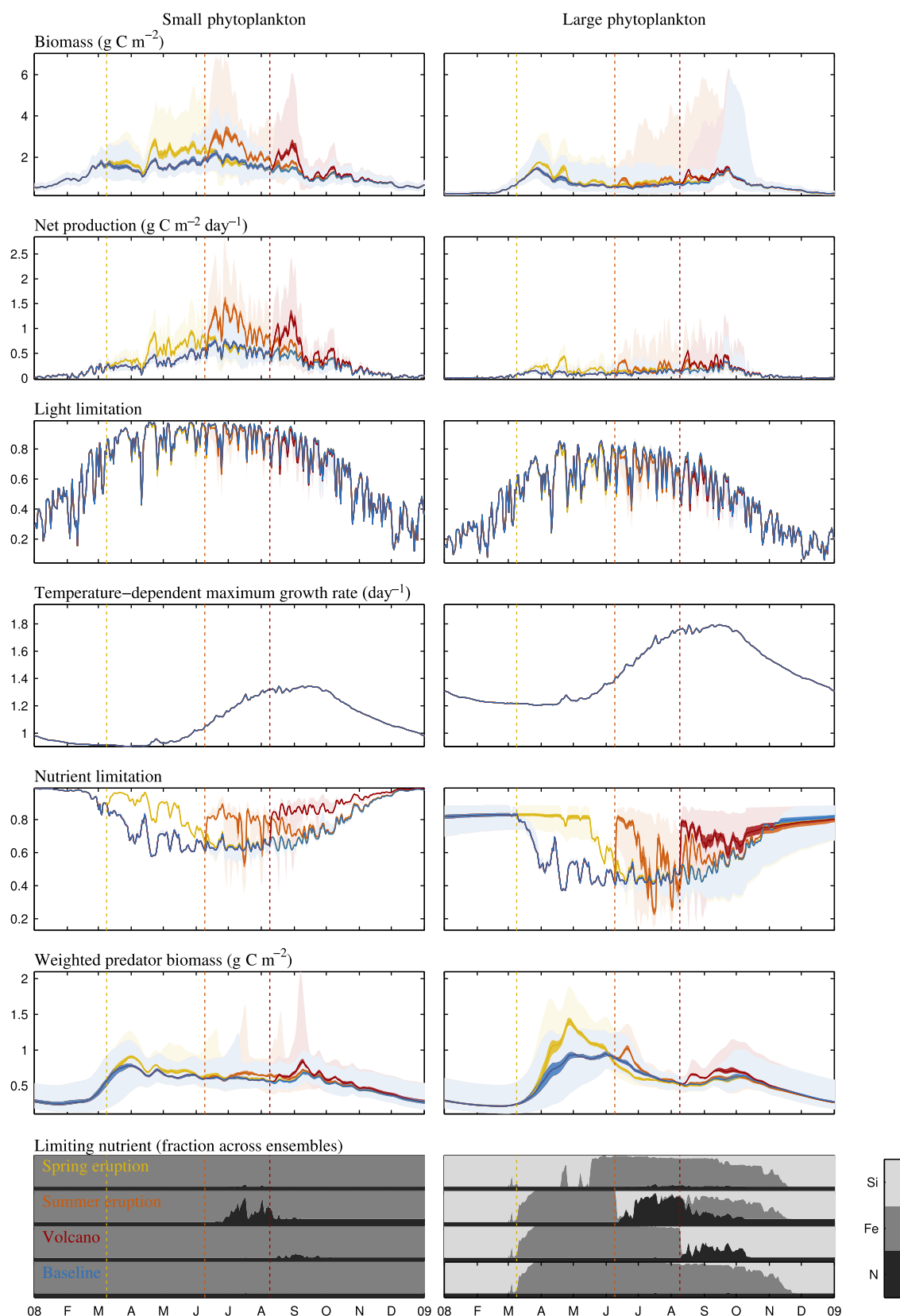


Figure 9. Phytoplankton biomass, net production, growth limitation terms, and weighted predator biomass (sum of all predators, weighted by fraction of mass-balanced diet composed of each phytoplankton group) for each phytoplankton group under the eruption timing scenarios. In the top panels, lines represent median values across ensembles, whereas lighter and darker shaded regions correspond to 0–100 and 40–60% ranges across ensembles, respectively. Vertical dotted lines indicate the timing of the three eruption scenarios. The bottom panels show the fraction of ensemble members limited by each nutrient under the four scenarios.

showing higher abundance of early copepodite stages of *E. bungii* and *N. plumchrus* (Tsuda *et al.*, 2005, 2006), as well as enhanced copepod growth (Tsuda *et al.*, 2006). Notably, in the no-diapause and late-diapause scenarios, most of this copepod production is diverted into the predatory zooplankton/chaetognath/sergestid shrimp groups, which generally dominate the zooplankton community in late summer and fall (Mackas, 1992), and the copepod biomass remains lower than baseline. Enhanced copepod or other mesozooplankton biomass in the other scenarios is consistent with Batten and Gower (2014) observations of a historically high crustacean zooplankton biomass three months after the fertilization event. Nevertheless, increases in simulated crustacean zooplankton production or biomass were never >30% of the baseline, and resulted in only a marginal increase in upper trophic level biomass, again highlighting how the high North

Pacific food web connectance limits the response of any specific group to iron fertilization.

A limitation of the modeling framework applied herein is that detailed life-cycle dynamics are not resolved. Highly variable survival responses during the immediate post-smolt period have been implicated as important drivers of fluctuation in salmon returns (Logerwell *et al.*, 2003). Parsons and Whitney (2012) posited that similar non-linearities acting on older, juvenile salmon may have accentuated the salmon response to Kasatochi. McKinnell (2013) argues that juvenile migration patterns for the Fraser River cohort of interest would place those particular salmon in the non-iron-limited coastal waters at the time of the eruption, so to truly address this aspect of the argument, resolution of migratory patterns may be necessary. However, it is notable that our simulated pelagic forage fish, which would have similar trophic characteristics to juvenile salmon, also

Figure 10. Fate of losses from each group along the pathway from nutrients to pink/sockeye salmon. Losses are categorized as either predatory losses to other groups on the nutrient-to-sockeye salmon pathway, predatory losses to groups off this pathway, fishing loss, and other non-predatory losses.

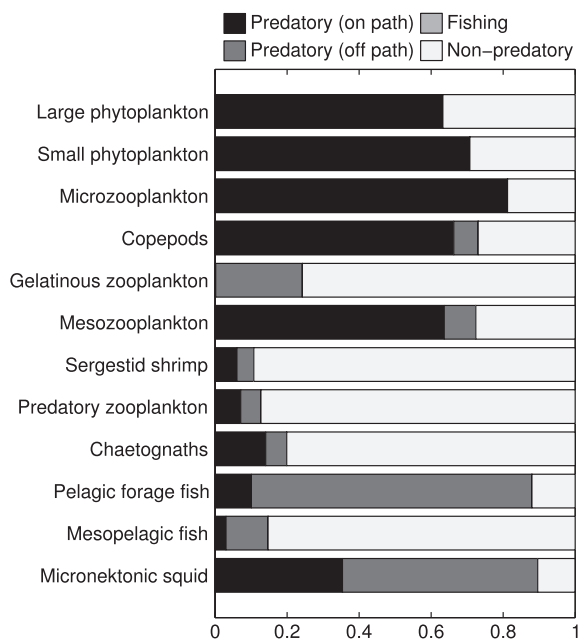
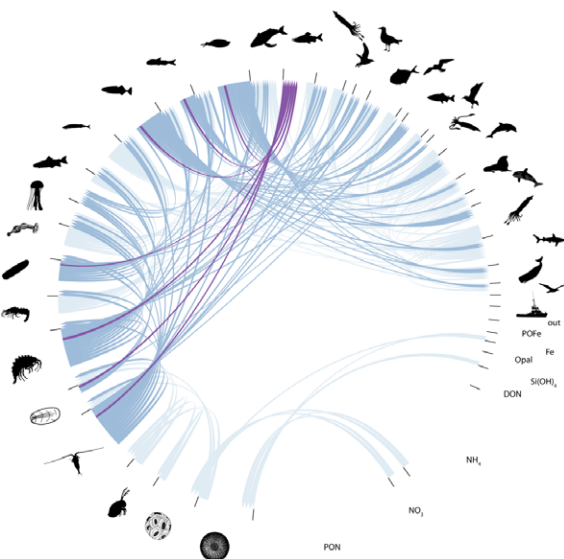


Figure 11. Pathways between sockeye salmon prey and all predators. Light blue edges indicate all links associated with primary production, grazing, and predation; purple edges are those leading to sockeye salmon from their prey groups; dark blue indicates all other predation links leading from those prey groups.



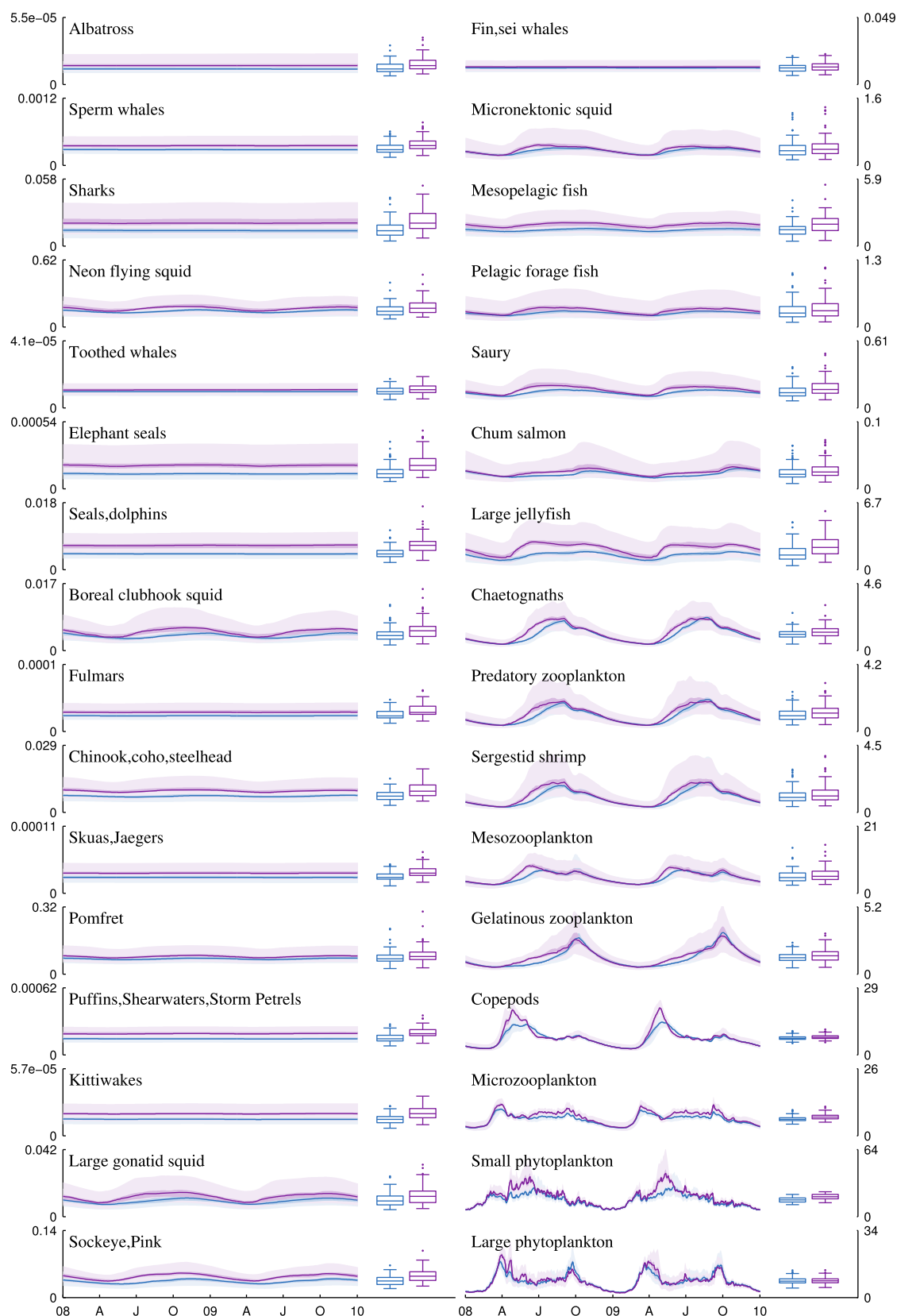


Figure 12. Timeseries of biomass under the baseline (blue) and constant-fertilization (purple) scenarios. Vertical axes are in units of mmol N m^{-2} and range from 0 to 4 times the median yearly biomass under baseline conditions for each functional group. Lines represent median values across ensembles, while lighter and darker shaded regions correspond to 10–90 and 40–60% ranges across ensemble members, respectively. Boxplots show the full range of yearly-averaged biomass values across all ensemble members.

show muted responses to the eruption owing to the high connectance within the food web. Further exploration of interactions between life cycle dynamics and the large-scale food web response analyzed herein is left to future work.

While the Kasatochi-like fall eruption scenario does not support the hypothesis that iron fertilization could greatly affect salmon biomass, the response of the food web to an eruption does appear to be seasonally-dependant. Eruptions occurring earlier in the growing season favor the crustacean zooplankton pathways, leading to the greatest net increase for almost all groups in the food web, including salmon. Later eruptions, even those occurring in mid-summer during the most favorable growing conditions and thus inducing the highest phytoplankton blooms, result in a smaller net effect at higher trophic levels since the less-efficient gelatinous zooplankton pathway is more strongly favored later in the year. While there are far fewer measurements of the gelatinous community than of crustacean mesozooplankton in the open ocean, the sparse observations seem to reflect the same seasonality as our model, with peak gelatinous zooplankton numbers occurring later in the year than the rest of the mesozooplankton community (Mackas, 1992), and the switch between high-energy zooplankton-based food chains and low-energy jellyfish-based food chains has been seen as a result of shifting plankton community composition after natural and anthropogenic disturbances of pelagic ecosystems (Greve and Parsons, 1977; Parsons and Lalli, 2002). The potential non-linearities in trophic transfer as a result of this shifting community composition suggest a need for better data constraints on the role of gelatinous zooplankton in this food web.

Artificial fertilization experiments led to similar biogeochemical responses near the location of fertilization (a region on order of 1000 km^2) as Kasatochi induced on the basin scale ($1.5\text{--}2.0 \times 10^6 \text{ km}^2$, Langmann *et al.*, 2010). Given that artificial fertilization affects a much smaller region than a volcanic fertilization event, and the already modest effects of short-term basin-scale volcanic fertilization, it is difficult to imagine that brief small-scale applications of iron could improve fisheries yield.

A natural next question is: how much of a difference could fertilization make over a longer time scale? To provide some insight, we ran the limiting case of no iron limitation (Fig. 12). In this scenario, the phytoplankton response is similar to the early spring eruption described above, with phytoplankton growth eventually limited by macronutrient limitation. With a consistent input of higher production over consecutive years, the food web response no longer requires an escape-the-predators window to benefit, and after 17 years of the new productivity regime, most upper trophic level species settle into new biomass values 30–50% higher than in the baseline conditions, with the largest beneficiaries being the top predators with no predatory losses. It is also important to note, however, that such a large-scale change in iron limitation would also effect the supply of nutrients to other ocean regions, with potential decreases in macronutrient levels in the subtropics (Sarmiento *et al.*, 2010).

Overall, the results herein suggest a limited (albeit not insignificant) impact of large-scale volcano-driven iron fertilization on North Pacific fish food webs. A modest increase in all Gulf-of-Alaska-reared salmon populations may be attributed to direct bottom-up impacts on growth, but the larger interannual variations in individual salmon stocks, such as the Fraser River sockeye salmon in 2010, are more likely a result of localized environmental factors affecting the recruitment and survival of each stock (McKinnell *et al.*, 2014).

ACKNOWLEDGEMENTS

This work was jointly funded by the National Marine Fisheries Service and the Climate Program Office of NOAA's office of Oceanic and Atmospheric Research. We thank Jorge Sarmiento, who provided valuable comments and suggestions throughout the analysis and write-up of this study. Several of the critter silhouettes used in the figures and tables of this paper were adapted from artwork by Eileen Kearney. The salinity state estimates were provided by the ECCO Consortium for Estimating the Circulation and Climate of the Ocean funded by the National Oceanographic

Partnership Program (NOPP). ECMWF ERA-Interim data used in this study have been obtained from the ECMWF data server.

REFERENCES

- Aita, M., Yamanaka, Y. and Kishi, M. (2003) Effects of ontogenetic vertical migration of zooplankton on annual primary production – using NEMURO embedded in a general circulation model. *Fish Oceanogr.* **12**:284–290.
- Aydin, K.Y., Myers, K.W. and Walker, R.V. (2000) Variation in summer distribution of the prey of Pacific salmon (*Oncorhynchus* spp.) in the offshore Gulf of Alaska in relation to oceanographic conditions, 1994–98. *North Pacific Anadromous Fish Comm. Bull.* **2**:43–54.
- Aydin, K.Y., McFarlane, G.A., King, J.R. and Megrey, B.A. (2003) The BASS/MODEL report on trophic models of the Subarctic Pacific Basin ecosystems. *PICES Sci. Rep.* **25**:1–93.
- Batten, S.D. and Gower, J.F.R. (2014) Did the iron fertilization near Haida Gwaii in 2012 affect the pelagic lower trophic level ecosystem. *J. Plankton Res.* **36**:925–932.
- Boyd, P. and Harrison, P.J. (1999) Phytoplankton dynamics in the NE subarctic Pacific. *Deep Sea Res. Part II Top. Stud. Oceanogr.* **46**:2405–2432.
- Boyd, P.W., Law, C.S., Wong, C.S. et al. (2004) The decline and fate of an iron-induced subarctic phytoplankton bloom. *Nature* **428**:549–553.
- Christensen, V. and Walters, C.J. (2004) Ecopath with Ecosim: methods, capabilities and limitations. *Ecol. Modell.* **172**:109–139.
- Denman, K.L. and Miyake, M. (1973) Upper layer modification at Ocean Station Papa: observations and simulation. *J. Phys. Oceanogr.* **3**:185–196.
- Denman, K., Voelker, C., Angelicapena, M. and Rivkin, R. (2006) Modelling the ecosystem response to iron fertilization in the subarctic NE Pacific: the influence of grazing, and Si and N cycling on CO₂ drawdown. *Deep Sea Res. Part II Top. Stud. Oceanogr.* **53**:2327–2352.
- Fan, S.M. and Dunne, J.P. (2011) Models of iron speciation and concentration in the stratified epipelagic ocean. *Geophys. Res. Lett.* **38**:15, L15611.
- Fan, S.M., Moxim, W.J. and Levy, H. (2006) Aeolian input of bioavailable iron to the ocean. *Geophys. Res. Lett.* **33**:2–5.
- Frost, B.W. (1987) Grazing control of phytoplankton stock in the open subarctic Pacific Ocean: a model assessing the role of mesozooplankton, particularly the large calanoid copepods *Neocalanus* spp. *Mar. Ecol. Prog. Ser.* **39**:49–68.
- Goldblatt, R., Mackas, D. and Lewis, A. (1999) Mesozooplankton community characteristics in the NE subarctic Pacific. *Deep Sea Res. Part II Top. Stud. Oceanogr.* **46**:2619–2644.
- Greve, W. and Parsons, T.R. (1977) Photosynthesis and fish production: hypothetical effects of climatic change and pollution. *Helgoländer Wiss. Meeresunters.* **30**:666–672.
- Hamme, R.C., Webley, P.W., Crawford, W.R. et al. (2010) Volcanic ash fuels anomalous plankton bloom in subarctic northeast Pacific. *Geophys. Res. Lett.* **37**:1–5.
- Johnson, K.S., Gordon, R. and Coale, K.H. (1997) What controls dissolved iron concentrations in the world ocean? *Mar. Chem.* **57**:137–161.
- Johnson, W.K., Miller, L.A., Sutherland, N.E. and Wong, C. (2005) Iron transport by mesoscale Haida eddies in the Gulf of Alaska. *Deep Sea Res. Part II Top. Stud. Oceanogr.* **52**:933–953.
- Kearney, K.A., Stock, C., Aydin, K. and Sarmiento, J.L. (2012) Coupling planktonic ecosystem and fisheries food web models for a pelagic ecosystem: description and validation for the subarctic Pacific. *Ecol. Modell.* **237–238**:43–62.
- Kearney, K.A., Stock, C. and Sarmiento, J.L. (2013) Amplification and attenuation of increased primary production in a marine food web. *Mar. Ecol. Prog. Ser.* **491**:1–14.
- Kishi, M., Motono, H., Kashiwai, M. and Tsuda, A. (2001) An ecological–physical coupled model with ontogenetic vertical migration of zooplankton in the northwestern Pacific. *J. Oceanogr.* **57**:499–507.
- Kishi, M., Kashiwai, M., Ware, D. et al. (2007) NEMURO – a lower trophic level model for the North Pacific marine ecosystem. *Ecol. Modell.* **202**:12–25.
- Langmann, B., Zaksiek, K., Hort, M. and Duggen, S. (2010) Volcanic ash as fertiliser for the surface ocean. *Atmos. Chem. Phys.* **10**:3891–3899.
- Logerwell, E., Mantua, N., Lawson, P., Francis, R. and Agostini, V. (2003) Tracking environmental processes in the coastal zone for understanding and predicting Oregon coho (*Oncorhynchus kisutch*) marine survival. *Fish Oceanogr.* **12**:554–568.
- Mackas, D. (1992) Seasonal cycle of zooplankton off southwestern British Columbia: 1979–89. *Can. J. Fish Aquat. Sci.* **49**:903–921.
- Mackas, D.L., Goldblatt, R. and Lewis, A.G. (1998) Interdecadal variation in developmental timing of *Neocalanus plumchrus* populations at Ocean Station P in the subarctic North Pacific. *Can. J. Fish Aquat. Sci.* **55**:1878–1893.
- McKinnell, S. (2013) Challenges for the Kasatoshi volcano hypothesis as the cause of a large return of sockeye salmon (*Oncorhynchus nerka*) to the Fraser River in 2010. *Fish Oceanogr.* **22**:337–344.
- McKinnell, S., Curchitser, E., Groot, K., Kaeriyama, M. and Trudel, M. (2014) Oceanic and atmospheric extremes motivate a new hypothesis for variable marine survival of Fraser River sockeye salmon. *Fish Oceanogr.* **23**:322–341.
- Miller, C.B., Frost, B.W., Batchelder, H.P., Clemons, M.J. and Conway, R.E. (1984) Life histories of large, grazing copepods in a subarctic ocean gyre: *Neocalanus plumchrus*, *Neocalanus cristatus*, and *Eucalanus bungii* in the Northeast Pacific. *Prog. Oceanogr.* **13**:201–243.
- Moore, J.K., Doney, S.C., Glover, D.M. and Fung, I.Y. (2002) Iron cycling and nutrient limitation patterns in surface waters of the World Ocean. *Deep Sea Res. Part II Top. Stud. Oceanogr.* **49**:463–507.
- Moore, J.K., Doney, S.C. and Lindsay, K. (2004) Upper ocean ecosystem dynamics and iron cycling in a global three-dimensional model. *Global Biogeochem. Cycles* **18**:n/a–n/a.
- Moxim, W.J., Fan, S.M. and Levy, H. (2011) The meteorological nature of variable soluble iron transport and deposition within the North Atlantic Ocean basin. *J. Geophys. Res.* **116**:1–26.
- Parsons, T.R. and Lalli, C.M. (2002) Jellyfish population explosions: revisiting a hypothesis of possible causes. *Mar.* **40**:111–121.

- Parsons, T.R. and Whitney, F.A. (2012) Did volcanic ash from Mt. Kasatoshi in 2008 contribute to a phenomenal increase in Fraser River sockeye salmon (*Oncorhynchus nerka*) in 2010? *Fish Oceanogr.* **21**:374–377.
- Polovina, J.J. (1984) Model of a coral reef ecosystem I. The ECOPATH model and its applications to French Frigate Shoals. *Coral Reefs* **3**:1–11.
- Sarmiento, J.L., Slater, R.D., Dunne, J., Gnanadesikan, A. and Hiscock, M.R. (2010) Efficiency of small scale carbon mitigation by patch iron fertilization. *Biogeosciences* **7**:3593–3624.
- Suzuki, K., Saito, H., Isada, T. et al. (2009) Community structure and photosynthetic physiology of phytoplankton in the northwest subarctic Pacific during an in situ iron fertilization experiment (SEEDS-II). *Deep Sea Res. Part II Top. Stud. Oceanogr.* **56**:2733–2744.
- Takeda, S. and Tsuda, A. (2005) An in situ iron-enrichment experiment in the western subarctic Pacific (SEEDS): introduction and summary. *Prog. Oceanogr.* **64**:95–109.
- Tollefson, J. (2012) Ocean-fertilization project off Canada sparks furore. *Nature* **490**:8–9.
- Tsuda, A., Kiyosawa, H., Kuwata, A. et al. (2005) Responses of diatoms to iron-enrichment (SEEDS) in the western subarctic Pacific, temporal and spatial comparisons. *Prog. Oceanogr.* **64**:189–205.
- Tsuda, A., Saito, H., Nishioka, J., Ono, T., Noiri, Y. and Kudo, I. (2006) Mesozooplankton response to iron enrichment during the diatom bloom and bloom decline in SERIES (NE Pacific). *Deep Sea Res. Part II Top. Stud. Oceanogr.* **53**:2281–2296.
- Uematsu, M., Wells, M.L., Tsuda, A. and Saito, H. (2009) Introduction to Subarctic iron Enrichment for Ecosystem Dynamics Study II (SEEDS II). *Deep Sea Res. Part II Top. Stud. Oceanogr.* **56**:2731–2732.
- Wong, C., Waser, N., Nojiri, Y. et al. (2002) Seasonal and interannual variability in the distribution of surface nutrients and dissolved inorganic carbon in the Northern North Pacific: influence of El Niño. *J. Oceanogr.* **58**:227–243.
- Xiu, P., Thomas, A.C. and Chai, F. (2014) Satellite bio-optical and altimeter comparisons of phytoplankton blooms induced by natural and artificial iron addition in the Gulf of Alaska. *Remote Sens. Environ.* **145**:38–46.

SUPPORTING INFORMATION

Additional Supporting Information may be found in the online version of this article:

Appendix S1. The Kearney ecosystem model.